

Evaluation of the performance of WRF9km in simulating climate over the upper Yellow River Basin

Yi-Jia LI^a, Xue-Jia WANG^{a,b,*}, Xiao-Hua GOU^{a,b}, Qi WANG^a, Tinghai OU^c, Guo-Jin PANG^d,
Mei-Xue YANG^e, Lan-Ya LIU^a, Li-Ya QIE^a, Tao WANG^a, Jia-Yu WANG^a, Si-Hao WEI^f,
Xiao-Lai CHENG^a

^a Key Laboratory of Western China's Environmental Systems (Ministry of Education), College of Earth and Environmental Sciences, Lanzhou University, Lanzhou 730000, China

^b Gansu Liancheng Forest Ecosystem Field Observation and Research Station, Lanzhou University, Lanzhou 730333, China

^c Regional Climate Group, Department of Earth Sciences, University of Gothenburg, Gothenburg 40530, Sweden

^d Faculty of Geomatics, Lanzhou Jiaotong University, Lanzhou 730070, China

^e Key Laboratory of Cryospheric Science and Frozen Soil Engineering, Northwest Institute of Eco-Environment and Resources, Chinese Academy of Sciences, Lanzhou 730000, China

^f School of Atmospheric Sciences, Sun Yat-sen University, Zhuhai 519082, China

Received 17 April 2024; revised 13 November 2024; accepted 4 December 2024

Abstract

Understanding the current climate in the Yellow River Basin is essential for accurately predicting future climate change and assessing its impacts on water resources and ecosystems; however, existing models exhibit notable biases in this region, primarily due to low resolution and errors in driving data and model domains. Using *in-situ* station observation data, CN05.1 gridded meteorological observation dataset, along with the ERA5 and MERRA2 reanalysis datasets, the performance of the WRF9km in simulating temperature and precipitation from 1980 to 2016 was comprehensively evaluated. Results indicate that the WRF9km model effectively captures the spatial pattern of air temperature, with a spatial correlation exceeding 0.86 (at the 95% confidence level) and a cold bias of -2.8 °C compared to CN05.1. This bias is primarily due to the underestimation of downward radiation and the overestimation of surface albedo. However, the WRF9km model fails to reproduce the observed warming trend across the entire region, especially during the summer. For precipitation, the WRF9km model generally reproduces the observed spatial pattern, with spatial correlation coefficients above 0.80 for all seasons except winter (at the 95% confidence level). However, the model overestimates precipitation relative to CN05.1 and underestimates it when compared to MERRA2. The precipitation bias is mainly attributed to the misrepresentation of wind fields and moisture by the WRF9km model. Regarding precipitation trends, different datasets yield divergent results, indicating substantial inter-annual variability that is difficult for the WRF9km to capture. Compared to the driving ERA5 data, the WRF9km model reduces cold biases between November and December, as well as wet biases across all seasons. The model also better simulates the winter warming trend in the western part of the UYRB and the summer wetting trend in the northern part. The evaluation of the WRF9km model provides valuable insights for the development of dynamical downscaling in terrain complex regions, especially for improving the surface albedo scheme and input driving data.

Keywords: WRF; Climate change; Upper Yellow River Basin; Air temperature; Precipitation

* Corresponding author. Key Laboratory of Western China's Environmental Systems (Ministry of Education), College of Earth and Environmental Sciences, Lanzhou University, Lanzhou, 730000, China.

E-mail address: wangxuejia@lzu.edu.cn (WANG X.-J.).

Peer review under responsibility of National Climate Centre (China Meteorological Administration).

<https://doi.org/10.1016/j.accre.2024.12.003>

1674-9278/© 2024 The Authors. Publishing services by Elsevier B.V. on behalf of KeAi Communications Co. Ltd. This is an open access article under the CC BY-NC-ND license (<http://creativecommons.org/licenses/by-nc-nd/4.0/>).

1. Introduction

Climate warming has become a focal point of worldwide attention and has had considerable effects on terrestrial, freshwater, cryosphere and coastal ecosystems, leading to increasingly irreversible losses (IPCC, 2022; Wang et al., 2022; Wee et al., 2023). Regional studies provide crucial insights into local climate changes and their impacts to effectively understand these challenges (Zhu et al., 2016; Lin et al., 2018; Giorgi, 2019).

A variety of regional climate models (RCMs) have been widely employed to simulate and project climate change in regions such as the Alps, America, Central and East Asia and the Tibetan Plateau (Wang et al., 2016; Lun et al., 2021; Niu et al., 2021; Liu et al., 2022). Research indicates that RCMs effectively capture the spatial distribution of temperature and precipitation in the Tibetan Plateau, improving the simulation of precipitation intensity and location by accurately reflecting terrain effects (Shi et al., 2011; Ji and Kang, 2013; Wang et al., 2013; Fu et al., 2021).

The Weather Research and Forecasting (WRF) model is an advanced mesoscale numerical weather prediction system designed for atmospheric research and forecasting applications. A recent study comparing the Regional Climate Model version 4 (RegCM4) and WRF at a 30 km horizontal resolution found that the WRF model outperforms RegCM4 in simulating annual average temperature and precipitation trends, demonstrating superior spatial pattern correlation (Gao, 2020). Another study, which assessed the performance of RCMs with a horizontal resolution of 30 km in simulating temperature extremes across China, indicated that WRF is more effective at capturing inter-annual variations in extreme indices (Kong et al., 2019). Overall, the WRF model achieves notable advancements in simulating climate elements in the complex regions of China, providing crucial technical support for regional climate change assessments.

RCMs are generally highly sensitive to different model configurations, such as domain size and horizontal resolution (Giorgi, 2019). In regions with steep terrain, selecting the appropriate horizontal resolution is crucial for regional climate simulations, particularly for accurately simulating precipitation and water vapour transport (Xu et al., 2018; Lin et al., 2018). Recent studies have indicated that a spatial resolution of 9 km, within the range of approximately 15–4 km (the so-called grey zone, where the cumulus parameterisation scheme can be tuned off), strikes a balance between detailed spatial simulation and computational costs (Shin and Hong, 2013; Lin et al., 2018). Ou et al. (2020) simulated the diurnal cycle of precipitation on the Tibetan Plateau using the WRF model with a 9 km resolution and found that experiments without the cumulus parameterisation scheme outperformed those that included it. Kilometre-scale modelling of the Tibetan Plateau can accurately reproduce the diurnal and seasonal cycles, lapse rates, spatial distribution of climate variables, precipitation frequency and intensity, as well as water vapour transport (Karki et al., 2019; Sugimoto et al., 2021). Additionally, domain configuration is crucial for climate simulations. Ou

et al. (2023) conducted regional downscaling over a broader domain extending to 50° N using the WRF model at a 9 km resolution (referred to as WRF9km), driven by the ERA5 reanalysis, and found that the WRF9km dramatically reduces the moisture bias in summer precipitation over the north-western Tibetan Plateau. Thus, high-resolution modelling and appropriate domain setting are vital to climate research, especially in the complex terrain of the Tibetan Plateau.

The upper Yellow River Basin (UYRB), characterised by a cold, semi-humid climate, is an irreplaceable water source for the mid and lower reaches of the Yellow River (Zhang et al., 2019), with its runoff accounting for nearly half of the total runoff in the entire basin (Lan et al., 2016). Between 1961 and 2020, the UYRB has witnessed an overall warming and humidification, with a temperature rise of 0.34 °C per decade and a precipitation increase of 9.3 mm per decade (Zhang et al., 2023). Projections from RCM simulations indicate considerable warming in high-altitude areas and an increased flood risk across the Yellow River Basin under a high greenhouse gas emission scenario (Wang et al., 2021a). Given the vulnerable ecosystem of the region, intricate climate dynamics and remarkable uncertainties in climate models, in-depth studies on climate change and simulations in the UYRB are urgently needed.

Existing models often exhibit deficiencies in simulating regional climate, particularly in terms of cold and wet biases, which can be attributed to errors in driving data, model domain configuration, the choice of physical parameterisation schemes and model resolution (Gu et al., 2020; Li et al., 2020; Prein et al., 2023). Additionally, several studies evaluating temperature performance do not consider the impact of station locations and topography on temperature biases. How does the WRF9km model perform in capturing the spatiotemporal distribution of climate in the UYRB when increasing resolution and expanding the model domain? What are the main causes of these biases? These questions should be addressed in this study. The findings of this study are expected to enhance our understanding of the evolution of the regional climate system, offering an important basis for water resource management and ecological protection.

2. Methods and data

2.1. Regional climate simulation experiment and the WRF9km dataset

This study used WRF simulations with a spatial resolution of 9 km (WRF9km), developed by Ou et al. (2023) from the Regional Climate Group at the University of Gothenburg, Sweden, to evaluate climate over the UYRB. The WRF model (version 3.7.1, developed by the National Center for Atmospheric Research, Boulder, CO, USA) employed a non-hydrostatic balance configuration (Skamarock et al., 2008) to dynamically downscale global reanalysis data, with the model domain centred over the Tibetan Plateau. The northern boundary of the model domain (8°–50° N, 65°–125° E) extended to 50°N, encompassing the core of the summer

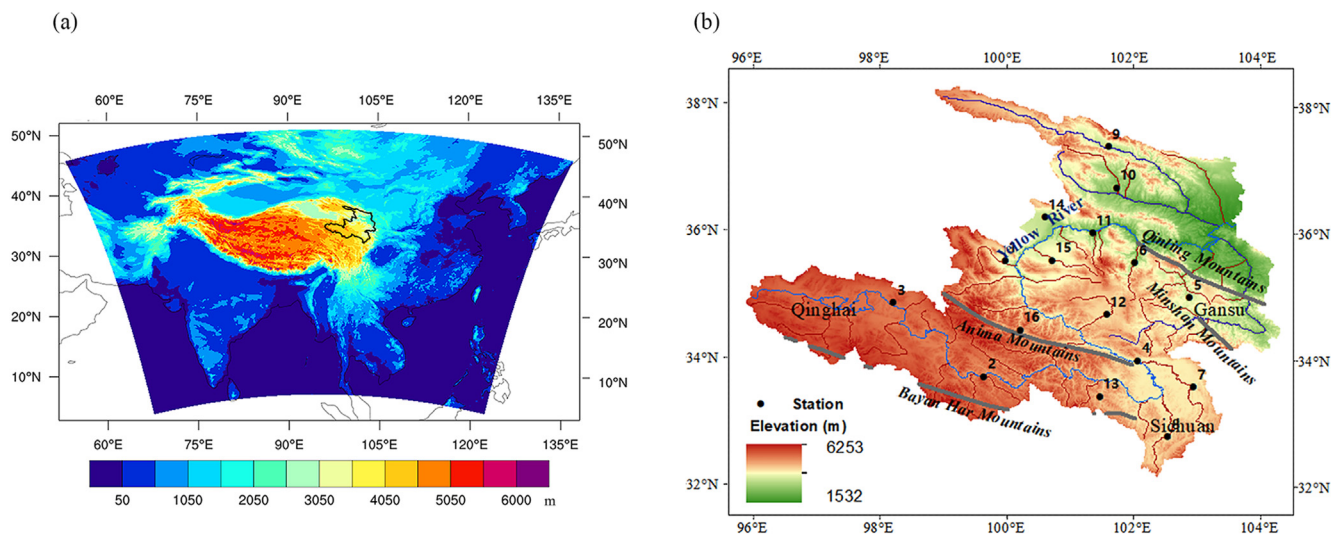


Fig. 1. Model domain (a) and topography and distribution of meteorological stations (b).

subtropical westerly jet in the upper troposphere (Fig. 1). The WRF9km experiment used the New Goddard shortwave radiation scheme, the RRTMG longwave radiation scheme (Iacono et al., 2008), the WRF Double Moment 6-class microphysics scheme, the unified Noah land surface model (Mukul Tewari et al., 2004) and the Yonsei University planetary boundary layer scheme (Hong et al., 2006). Two parallel, continuous simulations were simultaneously conducted to optimise computation time for long-term simulations, covering the periods 1979–1998 and 1998–2019. By analysing the overlapping year (1998) simulations, the differences in regional average precipitation, relative humidity, near-surface air temperature, surface skin temperature and surface net radiation between the two parallel simulations were relatively small. Therefore, the 1-year overlap strategy introduced minimal disturbance to the simulations, allowing the two simulations (1979–1998 and 1998–2019) to be merged into a continuous simulation covering the period from 1979 to 2019. The initial and boundary conditions were provided by ERA5 data, updated every 3 h, ensuring the timeliness and accuracy of the boundary conditions (Ou et al., 2023).

2.2. Validation data

The CN05.1 high-resolution gridded daily temperature and precipitation dataset was used as the reference data to assess the performance of the WRF9km in simulating near-surface air temperature and precipitation. CN05.1 is a meteorological dataset released by the China National Meteorological Information Center, generated by interpolating daily observations from 2416 national-level stations across mainland China. The dataset covers the period from January 1961 to the present, with a resolution of 0.25° , and covers the entire mainland of China (Wu and Gao, 2013). This dataset has been widely used for climate model validation and climate change studies (Miao and Wang (2020); Wang et al., 2021b). Additionally, *in-situ* station observational data provided by the

National Climate Centre of the China Meteorological Administration were used to validate model simulations at the station level (Appendix Table 1).

Temperature and precipitation data from the ERA5 reanalysis were used for comparison to assess the improvement of the WRF9km simulations. ERA5 has a spatial resolution of $0.25^\circ \times 0.25^\circ$ and a time period spanning from 1950 onwards (Muñoz-Sabater et al., 2021). The data is updated daily and undergoes monthly quality checks, during which preliminary products are replaced (Hersbach et al., 2020).

The Modern-Era Retrospective Analysis for Research and Applications, Version 2 (MERRA2), developed by the National Aeronautics and Space Administration, was used to identify the causes of temperature and precipitation biases in the WRF9km model. MERRA2 replaced the original MERRA reanalysis system by integrating the upgraded GEOS-5 data assimilation system and updating the model and global statistical interpolation schemes with a spatial resolution of $0.5^\circ \times 0.625^\circ$. MERRA2 contains meteorological variables such as radiation, albedo and water vapour transport, making it an important tool for understanding global climate change and evaluating climate model performance (Gelaro et al., 2017).

2.3. Evaluation strategy

The model simulations were collectively assessed for annual averages across four seasons: winter (December to February, DJF), spring (March to May, MAM), summer (June to August, JJA) and Autumn (September to November, SON). Bias, root mean square error (RMSE), correlation coefficient and linear trend between the WRF9km simulations and observations (CN05.1), as well as reanalysis data (ERA5, MERRA2), were compared to quantitatively evaluate model performance. The WRF9km simulations and reanalysis data (MERRA2) were interpolated onto a common grid resolution of $0.25^\circ \times 0.25^\circ$ to match that of CN05.1, ensuring

consistency. The common time period of 1980–2016 was also selected in the four datasets to conduct related analyses. Additionally, the WRF9km simulations and ERA5 were compared with 16 station observational data to mitigate potential biases arising from the relatively low number of stations used in most existing gridded datasets.

3. Results

3.1. Air temperature

As shown in Appendix Fig. A1 and Fig. 2, the spatial distribution of air temperature from the WRF9km simulation was compared with that from CN05.1, *in-situ* observations, ERA5 and MERRA2. Compared to CN05.1, the ERA5 data exhibited a noticeable warm bias in the central UYRB during all seasons and a cold bias in the southeast of the UYRB during DJF. The WRF9km model effectively captured the observed spatial distribution, with a high spatial correlation exceeding 0.97, particularly in JJA. Whilst the WRF9km

showed a warm bias in the northeast of the UYRB and a cold bias in other areas, it still demonstrated improvement by reducing the warm bias in the central region across all seasons, as well as the cold bias in the southeast during DJF, compared to ERA5. Notably, the spatial distribution of temperature in the MERRA2 data closely resembled CN05.1, with a spatial correlation greater than 0.98, making MERRA2 a suitable reference for analysing the sources of model bias.

As shown in Fig. 3a, compared to CN05.1, the regional mean ERA5 data displayed a large cold bias, except from June to September, during which it showed a slight warm bias. The WRF9km simulation consistently showed a cold bias throughout the year, relative to CN05.1 and the MERRA2 data, with the maximum bias occurring in April and May and the minimum in August. When compared to ERA5, the WRF9km data showed a reduction in the cold bias between November and December, indicating an improvement in the performance of the WRF9km model relative to its driving data. Compared to the observations from the 16 stations, the

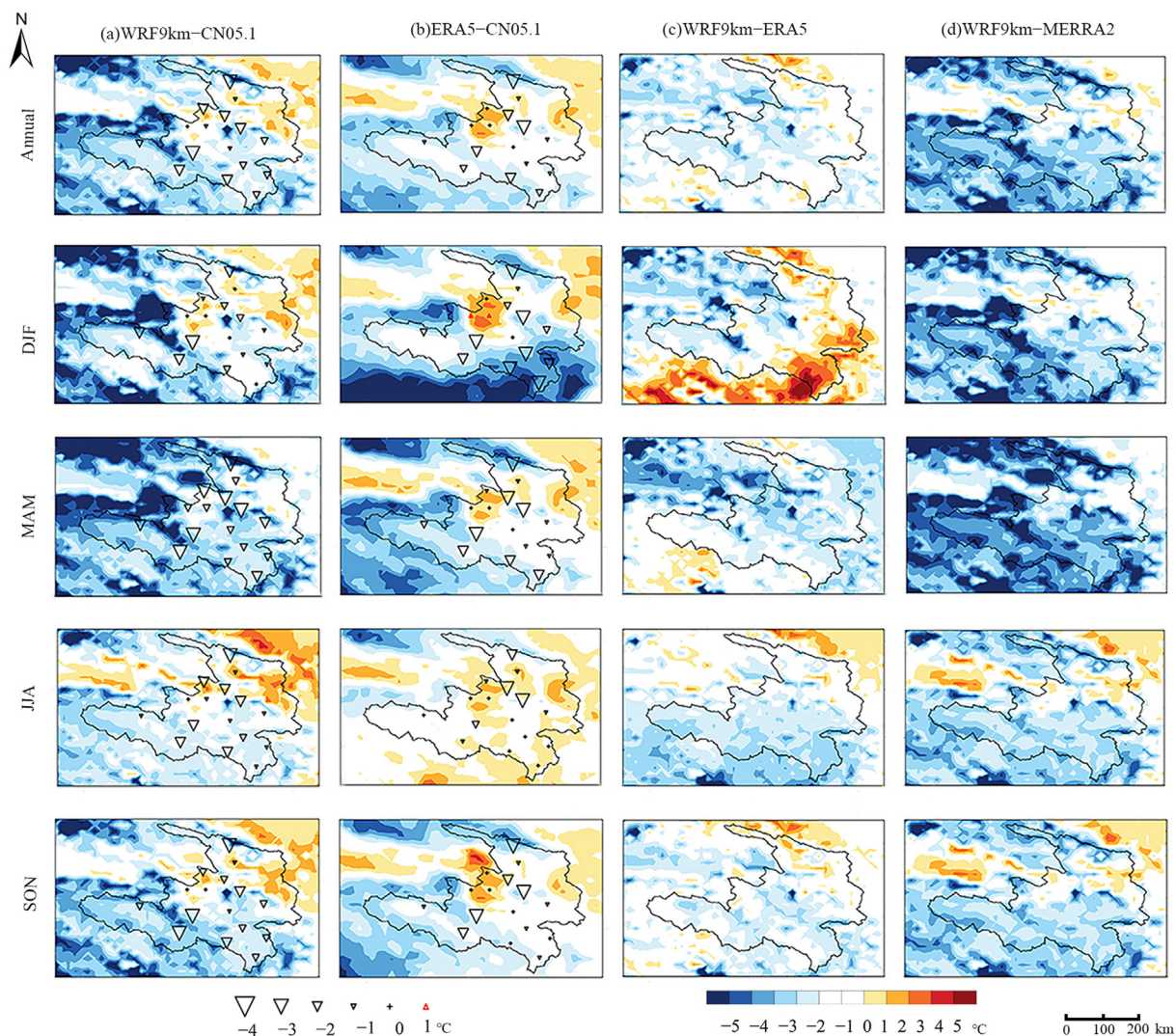


Fig. 2. Spatial distribution of temperature differences between WRF9km and CN05.1, ERA5 and CN05.1, WRF9km and ERA5 and WRF9km and MERRA2 from 1980 to 2016 (The symbols in (a) and (b) represent the temperature differences between WRF9km and ERA5 and the station data).

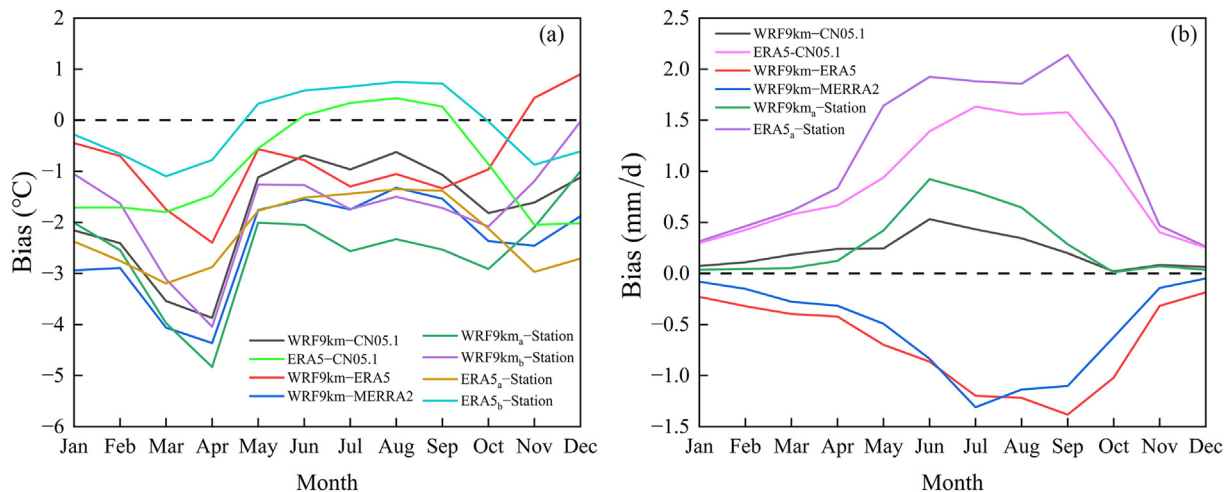


Fig. 3. Differences of air temperature (a) and precipitation (b) between WRF9km and reference data from 1980 to 2016 (WRF9km_a and ERA5_a represent the results of bilinear interpolation of WRF9km and ERA5 data at station location, respectively. WRF9km_b and ERA5_b represent the WRF9km_a and ERA5_a results after the lapse rate correction, respectively).

interpolated WRF9km simulations at these stations consistently exhibited a cold bias. This bias is primarily due to the fact that most observation stations are located in easily accessible valleys, whilst substantial elevation differences are found between the model grid cells and the observation stations. These topographic differences have a considerable impact on temperature in mountainous regions. A lapse rate of $0.65\text{ }^{\circ}\text{C}/(100\text{ m})$ was applied to correct the interpolated temperatures to address this issue, dramatically reducing the cold bias (Fig. 3a). Given the complex terrain of the UYRB, the climate simulation at 9 km does not fully resolve temperature at the station scale.

3.2. Precipitation

As shown in Fig. 3b, compared to CN05.1, the ERA5 considerably overestimated precipitation throughout the year. The WRF9km simulation also overestimated precipitation throughout the year, with the largest bias of 0.53 mm d^{-1} in June and the smallest bias of only 0.02 mm d^{-1} in October. In contrast, the WRF9km simulation underestimated precipitation for the entire year compared to ERA5, indicating that the WRF9km model largely mitigates the wet bias of ERA5.

As shown in Appendix Fig. A1 and Fig. 4, whether compared to CN05.1 or *in-situ* station data, the ERA5 data exhibited a remarkable wet bias. The WRF9km model satisfactorily captured the observed spatial pattern, with spatial correlations between the WRF simulations and the CN05.1/MERRA2 data generally exceeding 0.80 across all seasons except in DJF. However, precipitation was consistently overestimated by the WRF9km across the study area when compared to CN05.1, particularly in the southeastern region. In contrast, a noticeable underestimation of precipitation was observed across the entire region when compared to MERRA2. Overall, the WRF9km model showed the largest bias in JJA, whether compared to CN05.1 or MERRA2. In contrast, during DJF, when precipitation was at its lowest, the

model showed the smallest bias and RMSE despite lower correlation coefficients (Appendix Table A2). However, when compared to ERA5, the WRF9km data exhibited lower precipitation (Fig. 4c), indicating the WRF9km model effectively alleviated the wet bias in the ERA5 data.

3.3. Trend in air temperature

The observational results (CN05.1) revealed a notable upwards trend in regional average temperatures from 1980 to 2016 across all seasons (Fig. 5a). The most pronounced temperature increase occurred in DJF, with a trend of approximately $0.52\text{ }^{\circ}\text{C}$ per decade, which was statistically significant at the 95% level. The smallest increase was observed in SON, around $0.45\text{ }^{\circ}\text{C}$ per decade, also exceeding the 95% confidence threshold. In comparison, the WRF9km simulations consistently showed weaker warming trends across all seasons relative to CN05.1, especially in JJA. The temperature time series revealed a positive correlation between the WRF9km simulations and CN05.1, particularly during SON and DJF, with correlation coefficients of 0.80 and 0.50, respectively. This finding indicates that the model demonstrated superior performance in simulating inter-annual temperature variations during the colder seasons (SON and DJF). The WRF9km model exhibited a cold bias throughout the study period. Except for SON, the maximum cold bias occurred around 1990. The annual average and seasonal temperature biases showed a decreasing trend from 1980 to 2016, indicating that the temperature bias did not substantially improve over time. This trend may also explain the temperature bias observed in the spatial distribution.

The spatial distribution of temperature trends in the WRF9km simulations provided a clear representation of the model's performance in capturing spatial trend variations. As shown in Fig. 6, CN05.1, ERA5 and MERRA2 all showed a clear positive trend in annual and seasonal averages for the UYRB from 1980 to 2016. Compared to CN05.1, ERA5 showed an excessive warming trend in the central UYRB

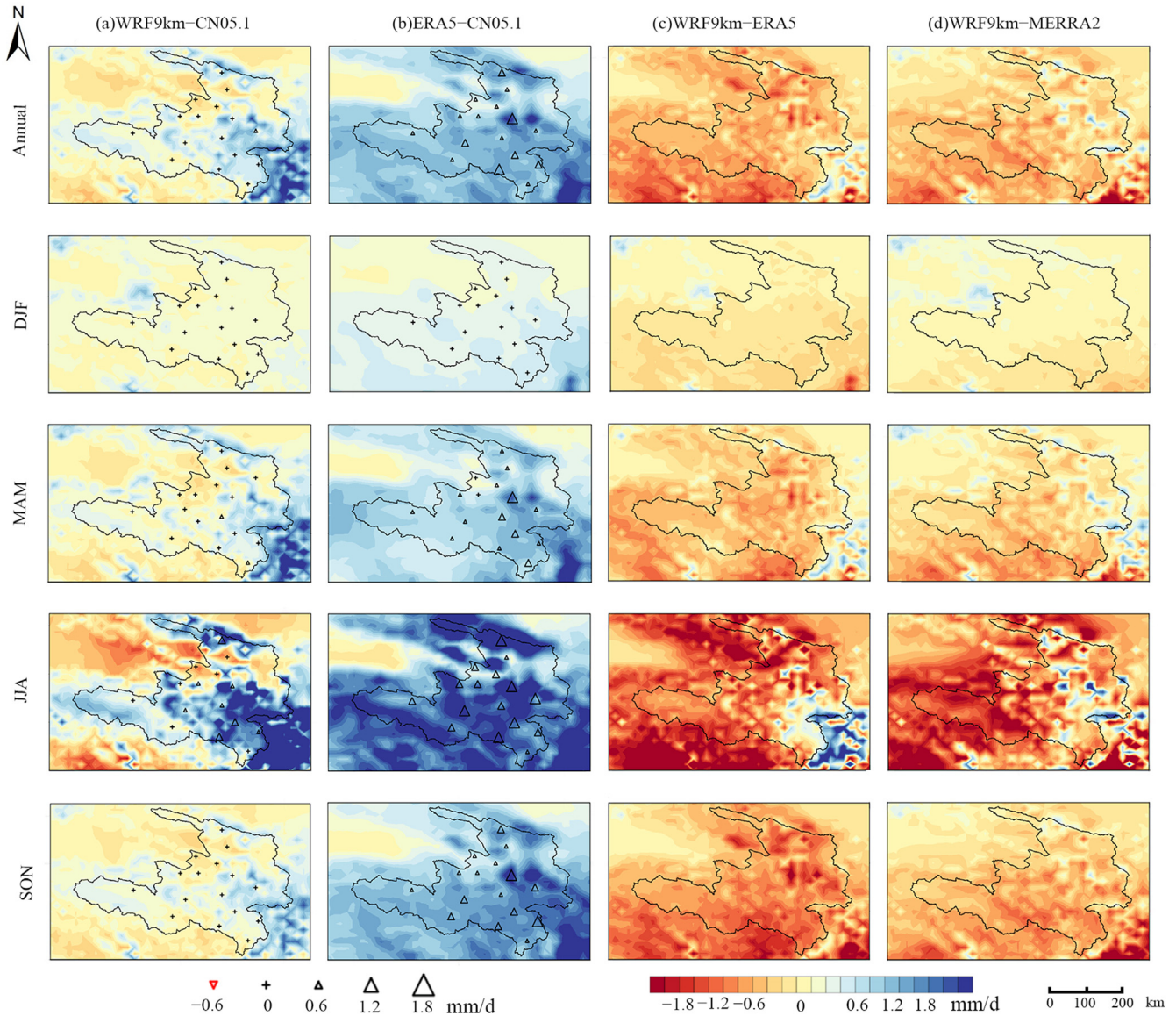


Fig. 4. Spatial distribution of precipitation differences between WRF9km and CN05.1, ERA5 and CN05.1, WRF9km and ERA5 and WRF9km and MERRA2 from 1980 to 2016 (The symbols in (a) and (b) represent the precipitation differences between WRF9km and ERA5 and the station data).

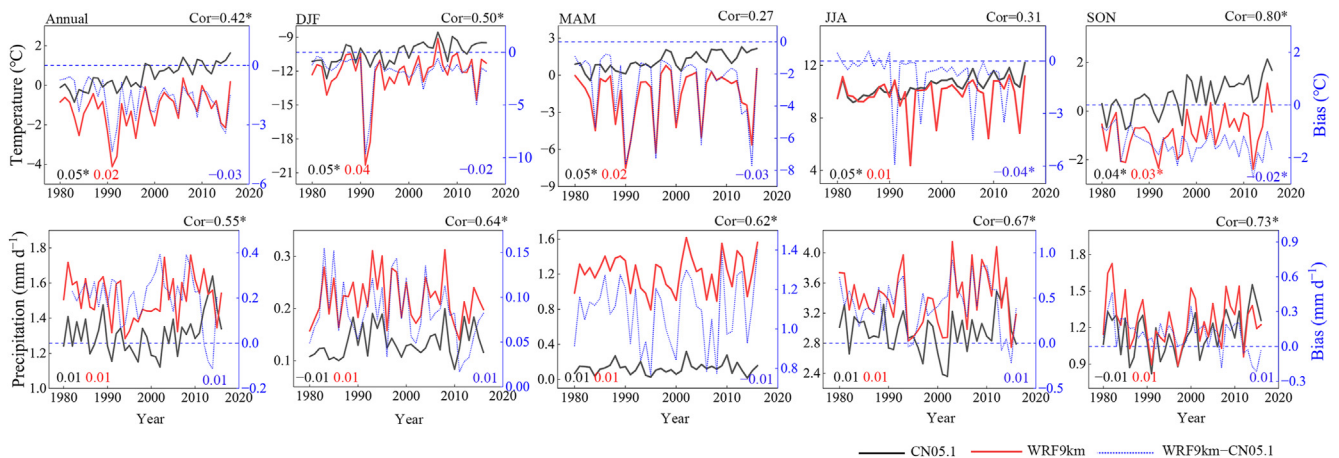


Fig. 5. Time series of annual and seasonal mean air temperature and precipitation from CN05.1 and WRF9km during 1980–2016, and the differences between WRF9km and CN05.1 (Numbers in the lower corner of the panels indicate trends in observed and simulated temperature (°C per decade) and precipitation (mm/d per decade). * denotes the correlation/trend exceeded the 0.05 significant level).

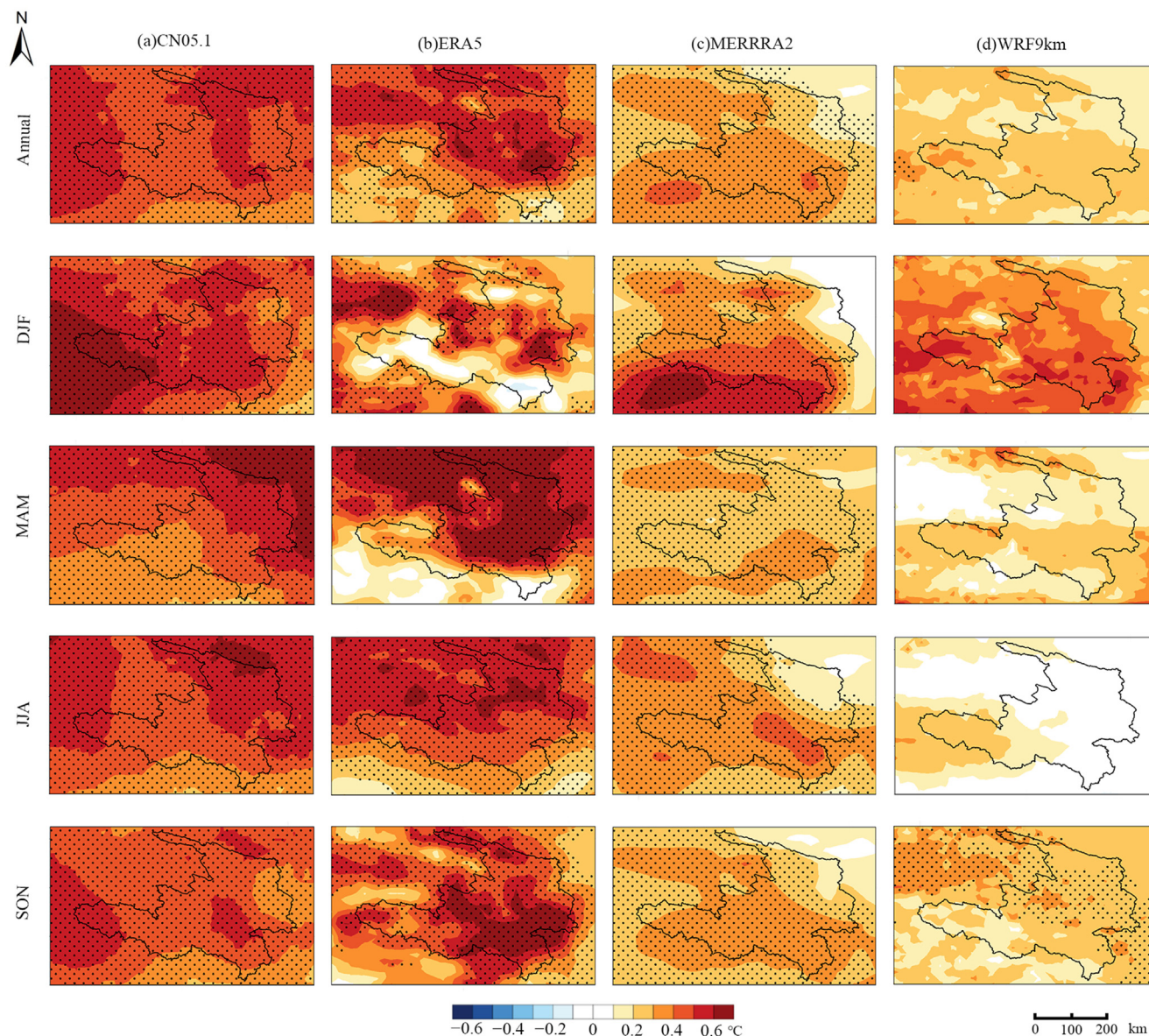


Fig. 6. Spatial distribution of linear trends in annual and seasonal mean air temperatures in the upper Yellow River Basin based on CN05.1, ERA5, MERRA2 data and WRF9km simulations from 1980 to 2016 (Black dots indicate that trends exceeds the 95% confidence level).

across all seasons, whilst no warming trend was observed in the southern UYRB during DJF. The WRF9km model also captured the warming trend, but differences existed in the spatial pattern and the magnitude of warming when compared to CN05.1 and MERRA2. CN05.1 displayed the maximum warming amplitude across all seasons, while the WRF9km model showed the smallest. The area with the maximum annual trend amplitude in CN05.1 was in the eastern and central UYRB, whereas in MERRA2 and WRF9km data, it was mainly concentrated in the southwestern region, except for the DJF period in the WRF9km simulation. However, compared to ERA5, the WRF9km model was able to enhance the weak warming trend in the southern UYRB during DJF

and reduce the overly strong warming trend in the central UYRB during the other seasons.

3.4. Trend in precipitation

As shown in Fig. 5b, the regional average precipitation in CN05.1 did not exhibit a considerable trend across all seasons. The WRF9km model performed well in simulating precipitation variability for the annual average and all four seasons, with correlation coefficients exceeding 0.55. Compared to CN05.1, the WRF9km model exhibited a remarkable wet bias, with the most pronounced one occurring in MAM, followed by JJA. Similar to temperature, no clear trend was observed in the

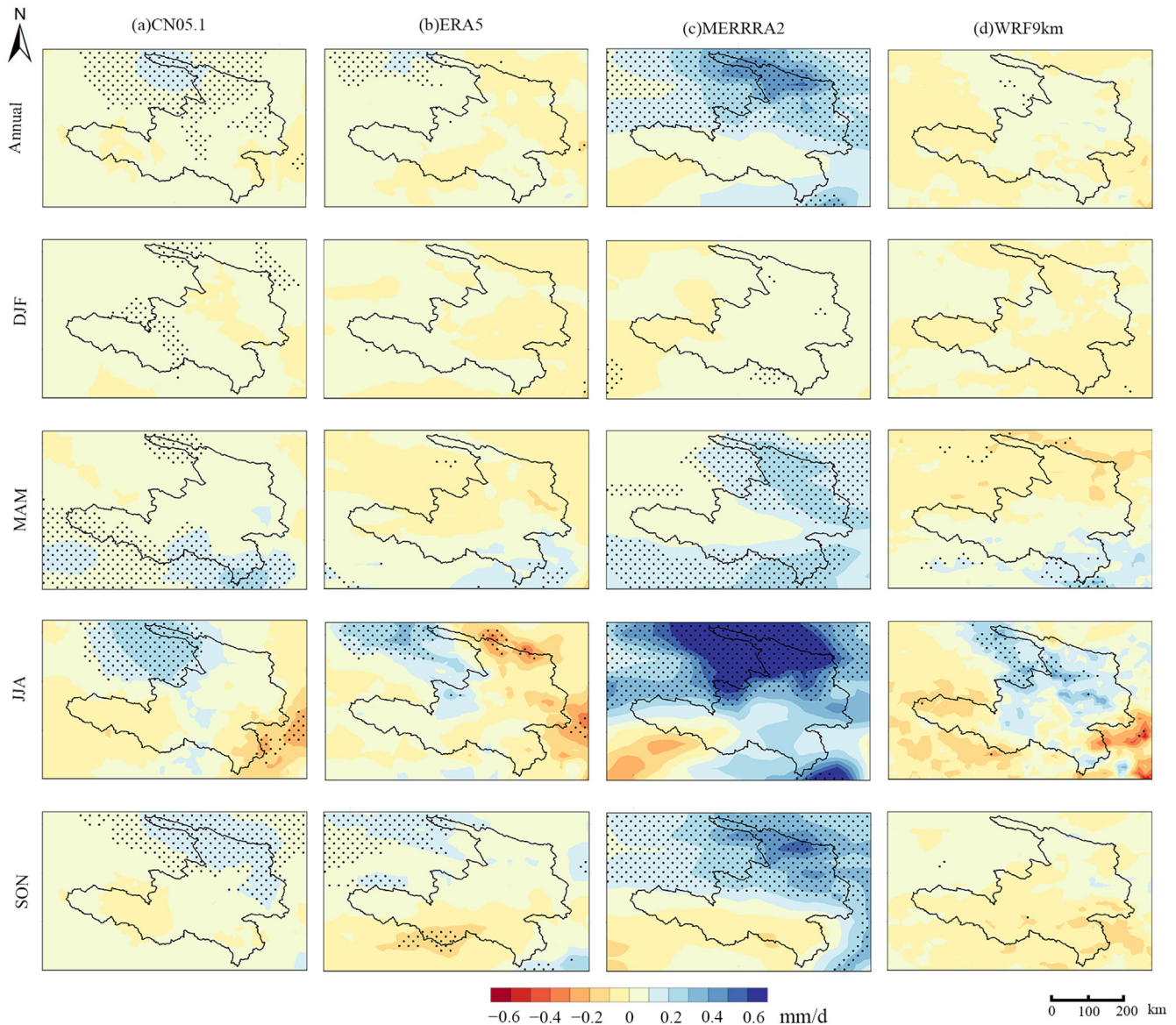


Fig. 7. Spatial distribution of linear trends in annual and seasonal mean precipitations in the upper Yellow River Basin based on CN05.1, ERA5, MERRA2 data and WRF9km simulations from 1980 to 2016 (Black dots indicate that trends exceeded the 95% confidence level).

precipitation bias from 1980 to 2016, indicating that the precipitation bias did not reduce over time.

As shown in Fig. 7, the trends in precipitation for the WRF9km simulation were generally consistent with those from ERA5 data and CN05.1 for the annual average, DJF and SON, despite some differences in the magnitude of the trends. For annual precipitation, CN05.1 and the WRF9km data showed no considerable trend in most regions. CN05.1 only presented an increasing trend in a small part of the northern region and a slightly decreasing trend sporadically in the southwestern UYRB. While the MERRA2 data exhibited a noticeable increasing trend in most of the northern region and a small part of the southern region, the changing trends for the four seasons varied across the different datasets, indicating a spatiotemporal variability in precipitation that is difficult for the WRF9km model to capture. In JJA, the ERA5 data

exhibited a discernible drying trend in the northeast part of the study area, while the WRF9km simulation indicated a moistening trend that closely matched CN05.1. This finding indicates that the WRF9km model reduced the bias in replicating the summer precipitation trend.

4. Discussion

4.1. Causes for air temperature bias

As shown in Fig. 8, the WRF9km simulation demonstrated a general negative bias in net downwards shortwave radiation (NSR) compared to the MERRA2 data. The warm (cold) temperature bias in JJA and SON largely corresponded to the positive (negative) net shortwave radiation in the WRF9km simulation. The WRF9km simulation showed an overall

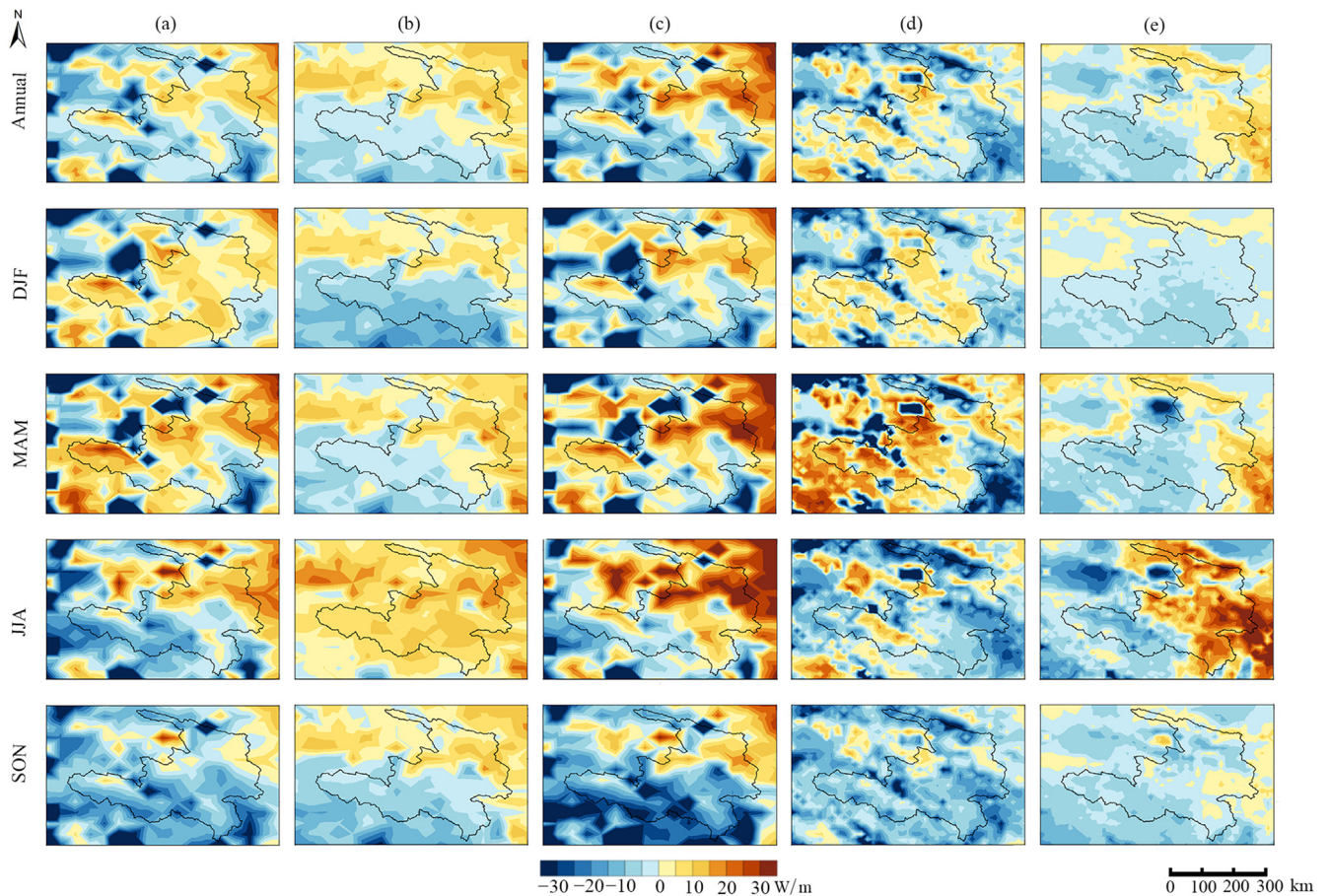


Fig. 8. Differences in (a) net shortwave radiation (NSR), (b) net longwave radiation (DLR), (c) net radiation forcing (NSR + DLR), (d) sensible heat flux and (e) latent heat flux between WRF9km and MERRA2 (WRF9km – MERRA2) over the upper Yellow River from 1980 to 2016.

negative downwards longwave radiation (DLR), but with positive values in the northeastern regions and overwhelming positive values across the UYRB in JJA, compared to the MERRA2 data. This pattern coincided with the warm bias, or a smaller bias, in temperature simulations in the northeastern area. The overestimation of downward longwave radiation (DLR) in JJA may be related to higher atmospheric moisture in the simulation, as discussed below. Additionally, the positive downwards longwave radiation (DLR) in the northeastern area and negative downwards longwave radiation (DLR) in the southwestern area counteracted some of the biases in net downwards shortwave radiation (NSR), resulting in a spatially uneven bias in downwards radiation forcing (NSR plus DLR) across the UYRB (Fig. 8c). The underestimation of downwards radiation forcing could help explain the cold bias in the WRF9km simulation.

The surface albedo between the WRF9km simulation and the MERRA2 data in the UYRB was compared to further investigate the cause of the shortwave radiation bias (Fig. 9). The analysis revealed that the albedo in the WRF9km simulation was generally overestimated in most areas of the UYRB, which contributed to the underestimation of NSR in the western UYRB in JJA and across the entire UYRB in SON. Another factor contributing to the NSR underestimation was

the overestimated downward shortwave radiation by the WRF9km (figure not shown), which was associated with lower precipitation compared to the MERRA2 data.

Additionally, the model bias may be influenced by the distribution of meteorological stations, especially in high-altitude areas. Meteorological stations are typically located in low-altitude valleys with high temperatures (Wang et al., 2016). Therefore, the high-altitude temperatures interpolated from these stations often include high-temperature values, resulting in a cold bias in the simulated values, especially in the source areas. This bias can be partially mitigated through topographic corrections.

4.2. Potential cause for precipitation bias

The comparisons of water vapour transport and moisture flux divergence were conducted at 500 and 200 hPa between the WRF9km simulation and the MERRA2 data to explain the potential reason for the simulated precipitation bias (Fig. 10–11). The direction and magnitude of water vapour flux and divergence portrayed by the WRF9km and MERRA2 data were generally consistent across the UYRB and surrounding regions for all four seasons, except during JJA. The MERRA2 and WRF9km data both showed eastward moisture transport in the

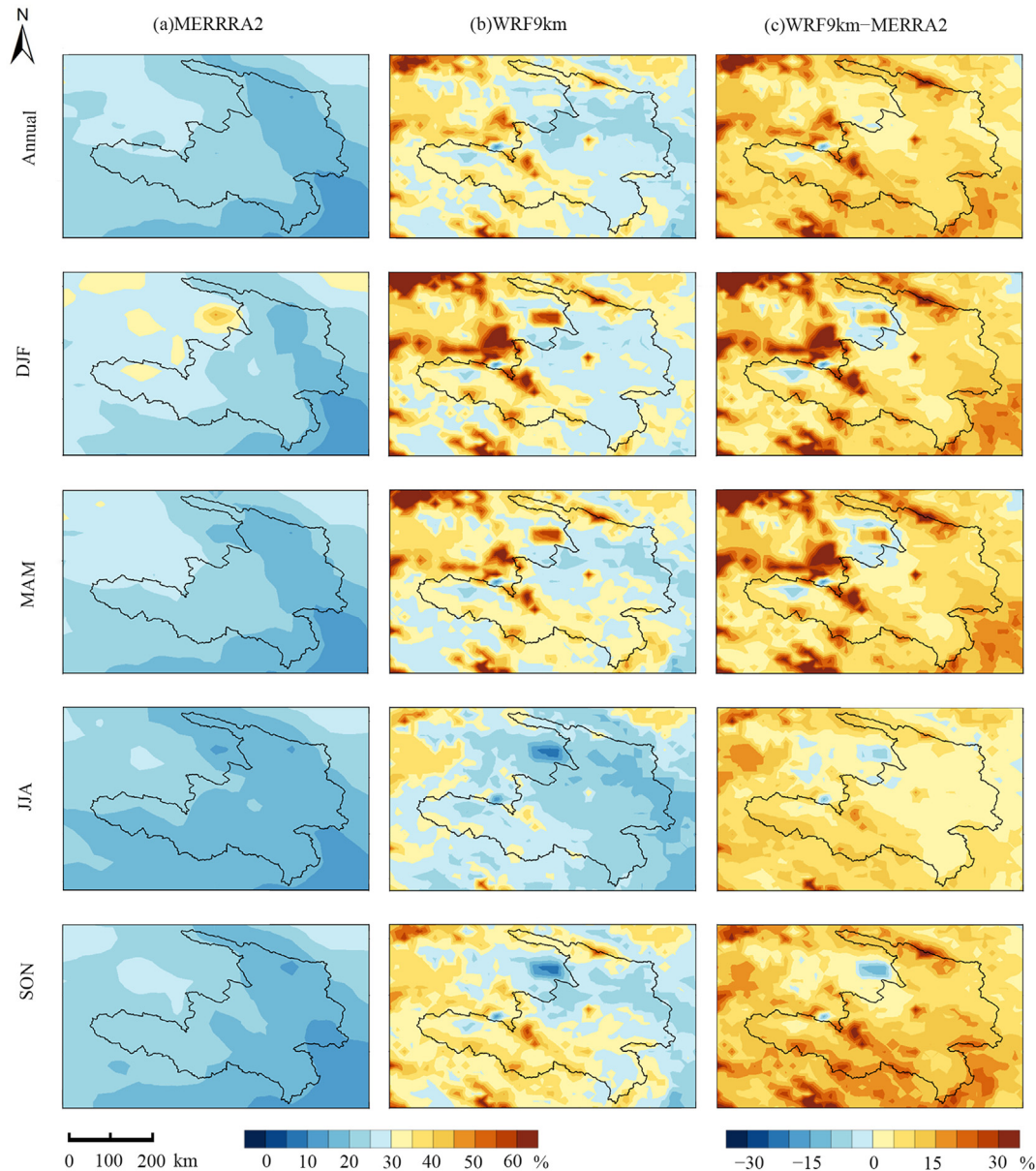


Fig. 9. Spatial distribution of annual and seasonal mean albedo from MERRA2 (a) and WRF9km (b), as well as their differences (c, WRF9km – MERRA2) from 1980 to 2016.

region dominated by the westerlies, which generally carry low moisture content, leading to reduced precipitation in MAM, SON and DJF. In JJA, with the onset and progression of the monsoon, moist air is transported from the Indian Ocean and the Pacific Ocean into the UYRB, contributing to higher precipitation. However, a considerable difference in moisture transport was observed between the WRF9km and the MERRA2 data in the southern part of the region. Whilst the MERRA2 data primarily showed southwest winds, the WRF9km simulated northwest winds. The northwest winds brought less moisture than the southwest winds, which accounts for the reduced precipitation in the WRF9km simulation compared to the MERRA2 data. Notably, in all seasons, the WRF9km simulated lower specific humidity at 500 hPa than MERRA2, leading to reduced precipitation in the simulation. The difference in

specific humidity at 500 hPa corresponded exactly to the precipitation bias between both datasets, showing larger dry biases in JJA and SON and smaller biases in other seasons.

At 200 hPa, the MERRA2 and WRF9km data indicated that moisture transport over the UYRB and surrounding regions was primarily eastward (Fig. 11). Compared to the water vapour transport at 500 hPa, the eastward moisture transport at 200 hPa was more pronounced over the UYRB. This process contributed less to overall precipitation due to the limited moisture flux in the northwest inland region. The dry bias in the WRF9km simulation, relative to the MERRA2 data, can be attributed to the stronger northwest water vapour transport and lower humidity. The wet bias, in contrast to CN05.1, may also be linked to inaccuracies in the wind fields and moisture representation within the WRF9km simulation.

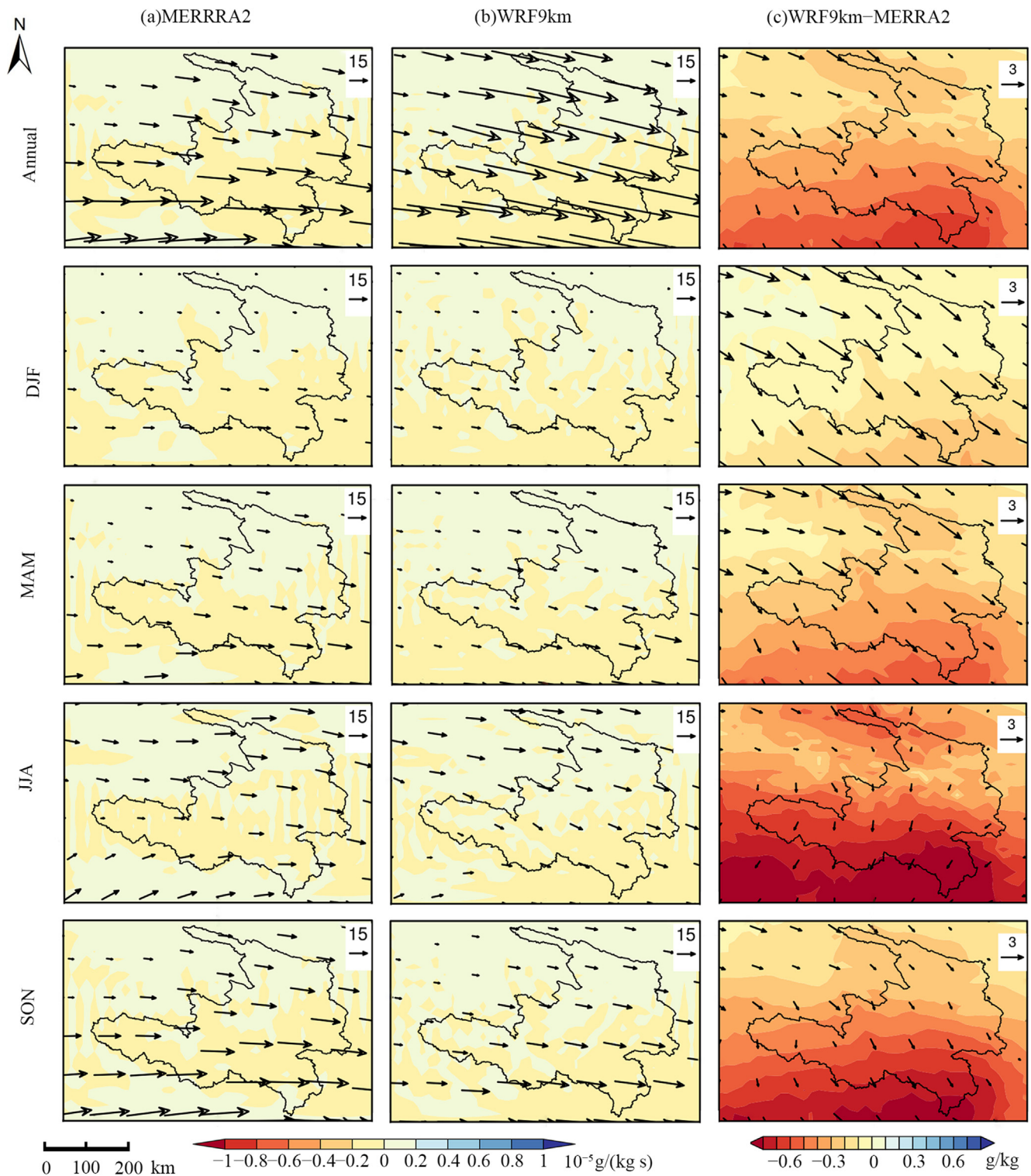


Fig. 10. Spatial distribution of water vapour transport at 500 hPa (vector, $\text{g}/(\text{kg}) (\text{m}/\text{s})$) and moisture flux convergence (shade) from MERRA2 and WRF9km and the differences in winds (vector, m/s) and specific humidity (shade, g/kg) between WRF9km and MERRRA2 from 1980 to 2016.

However, despite these explanations, no atmospheric variables were available to directly correlate with the observed precipitation variations.

Local convective activity also plays a crucial role in precipitation (Wang et al., 2016; Kukulies et al., 2020). Fig. 8d–e

compared surface turbulent fluxes between the WRF9km and MERRA2 data. In most areas of the study region, the WRF9km simulated latent heat flux was lower than that of MERRA2, except in JJA, indicating that weaker water vapour evaporation contributed to reduced precipitation in this region.

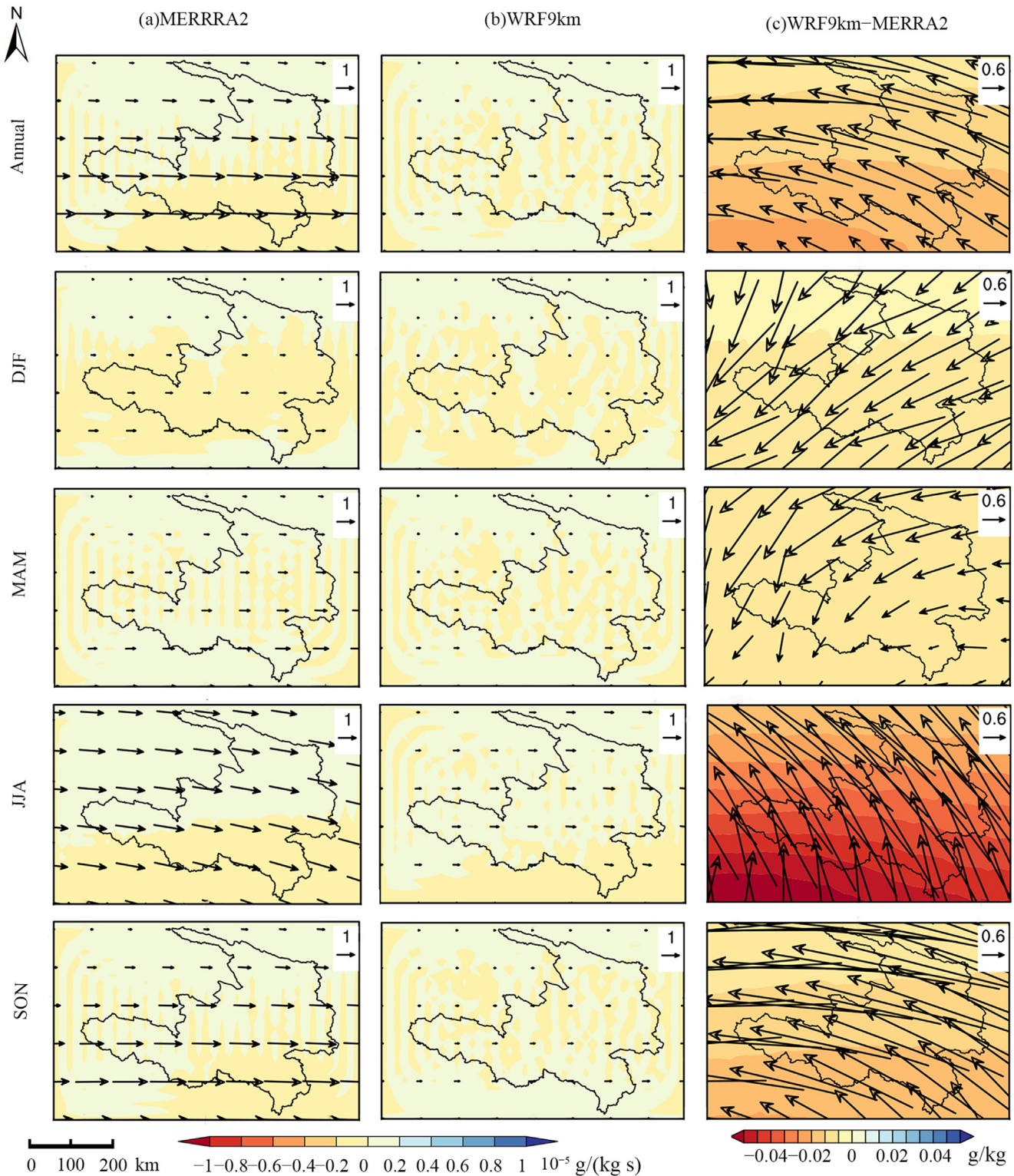


Fig. 11. Spatial distribution of water vapour transport at 200 hPa (vector, $(\text{g/kg}) (\text{m/s})$) and moisture flux convergence (shade) from MERRA2 and WRF9km and the differences in winds (vector, m/s) and specific humidity (shade, g/kg) between WRF9km and MERRRA2 from 1980 to 2016.

The WRF9km also simulated a weaker sensible heat flux in most areas of the UYRB, except in DJF and MAM, compared to the MERRA2 data. The reduced sensible heat flux led to a lower turbulent heat exchange between the atmosphere and the

underlying surfaces, which may have resulted in less convective precipitation in the WRF9km simulation. This factor contributes to the dry bias observed in the WRF9km simulation model.

4.3. Limitations and uncertainties

This study shows that with improvements in model resolution and the expansion of the model domain, the WRF9km model exhibits remarkable improvements in cold and wet biases. However, considerable shortcomings remain in capturing the spatial variation trends of temperature and precipitation. Simply increasing the model resolution and expanding the model domain is still insufficient; further improvements are necessary in the driving data and physical parameterisation schemes. The continuous improvement in numerical model resolution implies the increasing need to address a growing number of small-scale processes (*e.g.* local convection and turbulence), which often exhibit inherent nonlinearity and non-Gaussian characteristics (Carrassi et al., 2018). Transitioning to higher-resolution models will likely require corresponding developments in data assimilation techniques (Carrassi et al., 2018). A promising avenue will involve the integration of observational data with model simulations to reduce model uncertainty through data assimilations.

The evaluation of the WRF9km simulations in the UYRB only focused on air temperature and precipitation. Additional variables, such as soil temperature and moisture (Hasan et al., 2023), as well as land–atmosphere interactions, will be comprehensively validated to comprehensively explore the applicability of the WRF9km simulations and the mechanisms of climate change in the UYRB. Considerable biases in the simulation of convective processes are observed in the explanation of precipitation mechanisms. Further investigation into the impact of high mountains on the westerlies and the Asian summer monsoon, as well as their interactions, is needed through high-resolution climate simulations and high-precision observational datasets to enhance the understanding of the driving mechanisms of precipitation in the UYRB (Ou et al., 2023). Specifically, analysing the causes of the wet bias is necessary due to data limitations on water vapour transport in the CN05.1. Therefore, this study indirectly uses MERRA2 as a reference to analyse the physical processes for model biases. However, some uncertainties remain in MERRA2, as it is generated by assimilating observational data with numerical models. The quality of MERRA2 data is inevitably influenced by factors such as model resolution, data sources, data assimilation methods and boundary conditions.

4.4. Future outlook

Considering atmospheric circulation and local convection, enhancing the simulation of water vapour transport processes is necessary to further improve the simulation accuracy of the WRF9km model, especially precipitation. Additionally, in simulating inter-annual variations, particularly in MAM and JJA, the WRF9km model exhibits remarkable bias in the magnitude of precipitation trend. Future studies should focus on optimising physical parameterisation schemes and improving driving data to effectively simulate inter-annual precipitation variability. Moreover, incorporating high-

resolution observational data (particularly variables related to water vapour transport), along with data assimilation techniques, will help reduce model uncertainties. When applying RCMs in other regions, implementing tailored adjustments that accurately reflect the unique climate characteristics and diverse topography of those areas.

5. Conclusions

The WRF9km climate simulations in the UYRB were assessed from 1980 to 2016. The WRF9km model performed reasonably well in the spatial temperature pattern, with a spatial correlation coefficient exceeding 0.86, despite a cold bias of over -2.8 °C. The cold bias may be associated with the downward radiation bias and an overestimated albedo. Correcting the topographic effect using the temperature lapse rate could help alleviate the cold bias in the UYRB in the WRF9km model.

The WRF9km roughly reproduced the spatial pattern of precipitation despite exhibiting biases different from those of the reference data. Compared to CN05.1, the WRF9km simulation showed a wet bias across most areas of the UYRB during all seasons except DJF. Comparisons with MERRA2 data indicated that the model's representation of humidity and moisture transport plays a crucial role in the precipitation bias.

The warming trend simulated by the WRF9km model was relatively weak compared to CN05.1. The inter-annual variations in regionally averaged precipitation simulated by the WRF9km generally aligned with the observational data, except for MAM and JJA; however, discrepancies in magnitude were noted. Therefore, whilst the WRF9km model is somewhat effective in capturing inter-annual trends, considering different seasons and trend intensities, its accuracy can still be improved, particularly when simulating the magnitudes of temperature and precipitation changes.

Compared to CN05.1, the WRF9km model effectively alleviates the cold bias in ERA5 during November and December. In terms of precipitation, the WRF9km data notably reduces the wet biases observed in ERA5 data across all seasons. Additionally, the WRF9km data corrects the excessive warming trend in the central UYRB, which is evident in ERA5 data throughout all seasons. Furthermore, the WRF9km data depicts a moistening trend in the northeast part of the UYRB during JJA, a trend that ERA5 fails to capture. This trend indicates that the WRF9km model has an enhanced capability to reproduce JJA precipitation trends.

Declaration of competing interest

The authors declare that they have no known competing financial interests or personal relationships that could have appeared to influence the work reported in this paper.

CRedit authorship contribution statement

Yi-Jia Li: Writing – original draft, Formal analysis, Data curation. **Xue-Jia Wang:** Writing – review & editing,

Supervision. **Xiao-Hua Gou:** Conceptualization. **Qi Wang:** Validation, Conceptualization. **Tinghai Ou:** Writing – review & editing. **Guo-Jin Pang:** Formal analysis. **Mei-Xue Yang:** Writing – review & editing. **Lan-Ya Liu:** Software. **Li-Ya Qie:** Data curation. **Tao Wang:** Visualization. **Jia-Yu Wang:** Data curation. **Si-Hao Wei:** Visualization. **Xiao-Lai Cheng:** Data curation.

Acknowledgments

This study was jointly financed by the National Natural Science Foundation of China (42161025, U21A2006, 42477483, 42442055), the Young Doctor Support Project of Education Department of Gansu Province (2023QB-060), and the Start-up Funds for Introduced Talent at Lanzhou University (561120217). This work was supported by the Super-computing Center of Lanzhou University.

Appendix A. Supplementary data

Supplementary data to this article can be found online at <https://doi.org/10.1016/j.accre.2024.12.003>.

References

- Carrassi, A., Bocquet, M., Bertino, L., et al., 2018. Data assimilation in the geosciences: an overview of methods, issues, and perspectives. *Wires Clim. Change* 9 (5), e535. <https://doi.org/10.1002/wcc.535>.
- Fu, Y.H., Gao, X.J., Zhu, Y.M., et al., 2021. Climate change projection over the Tibetan Plateau based on a set of RCM simulations. *Adv. Clim. Change Res.* 12 (3), 313–321. <https://doi.org/10.1016/j.accre.2021.01.004>.
- Gao, S., 2020. Dynamical downscaling of surface air temperature and precipitation using RegCM4 and WRF over China. *Clim. Dynam.* 55 (5–6), 1283–1302. <https://doi.org/10.1007/s00382-020-05326-y>.
- Gelaro, R., McCarty, W., Suárez, M.J., et al., 2017. The Modern-Era Retrospective analysis for research and applications, version 2 (MERRA-2). *J. Clim.* 30 (14), 5419–5454. <https://doi.org/10.1175/jcli-d-16-0758.1>.
- Giorgi, F., 2019. Thirty years of regional climate modeling: where are we and where are we going next? *J. Geophys. Res. Atmos.* 124 (11), 5696–5723. <https://doi.org/10.1029/2018jd030094>.
- Gu, H., Yu, Z., Peltier, W.R., et al., 2020. Sensitivity studies and comprehensive evaluation of RegCM4.6.1 high-resolution climate simulations over the Tibetan Plateau. *Clim. Dynam.* 54 (7–8), 3781–3801. <https://doi.org/10.1007/s00382-020-05205-6>.
- Hersbach, H., Bell, B., Berrisford, P., et al., 2020. The ERA5 global reanalysis. *Q. J. R. Meteorol. Soc.* 146, 1999–2049. <https://doi.org/10.1002/qj.3803>.
- Hong, S.Y., Noh, Y., Dudhia, J., 2006. A new vertical diffusion package with an explicit treatment of entrainment processes. *Mon. Weather Rev.* 134 (9), 2318–2341. <https://doi.org/10.1175/MWR3199.1>.
- Hasan, M.A., Mia, M.B., Khan, M.R., et al., 2023. Temporal changes in land cover, land surface temperature, soil moisture, and evapotranspiration using remote sensing techniques: a case study of kutupalong Rohingya refugee camp in Bangladesh. *J. Geovis. Spatial Anal.* 7 (1), 1–22. <https://doi.org/10.1007/s41651-023-00140-6>.
- Iacono, M.J., Delamere, J.S., Mlawer, E.J., et al., 2008. Radiative forcing by long-lived greenhouse gases: calculations with the AER radiative transfer models. *J. Geophys. Res. Atmos.* 113, D13103. <https://doi.org/10.1029/2008jd009944>.
- IPCC, 2022. *Climate Change 2022: Impacts, Adaptation, and Vulnerability. Contribution of Working Group II to the Sixth Assessment Report of the Intergovernmental Panel on Climate Change.* Cambridge University Press, Cambridge and New York. <https://doi.org/10.1017/9781009325844>.
- Ji, Z., Kang, S., 2013. Double-nested dynamical downscaling experiments over the Tibetan Plateau and their projection of climate change under two RCP scenarios. *J. Atmos. Sci.* 70 (4), 1278–1290. <https://doi.org/10.1175/jas-d-12-0155.1>.
- Karki, R., Hasson, S.u., Schickhoff, U., et al., 2019. Near surface air temperature lapse rates over complex terrain: a WRF based analysis of controlling factors and processes for the central Himalayas. *Clim. Dynam.* 54 (1–2), 329–349. <https://doi.org/10.1007/s00382-019-05003-9>.
- Kong, X., Wang, A., Bi, X., et al., 2019. Assessment of temperature extremes in China using RegCM4 and WRF. *Adv. Atmos. Sci.* 36 (4), 363–377. <https://doi.org/10.1007/s00376-018-8144-0>.
- Kukulies, J., Chen, D., Wang, M., 2020. Temporal and spatial variations of convection, clouds and precipitation over the Tibetan Plateau from recent satellite observations. Part II: precipitation climatology derived from global precipitation measurement mission. *Int. J. Climatol.* 40 (11), 4858–4875. <https://doi.org/10.1002/joc.6493>.
- Lan, Y., Zhu, Y., Liu, G., et al., 2016. Seasonal characteristics and regional differences of climate change in the Yellow River source area. *J. Glaciol.* 38 (3), 741–749. <https://doi.org/10.7522/j.issn.1000-0240.2016.0083> (Chinese).
- Li, P., Furtado, K., Zhou, T., et al., 2020. Convection-permitting modelling improves simulated precipitation over the central and eastern Tibetan Plateau. *Q. J. R. Meteorol. Soc.* 147 (734), 341–362. <https://doi.org/10.1002/qj.3921>.
- Lin, C., Chen, D., Yang, K., et al., 2018. Impact of model resolution on simulating the water vapor transport through the central Himalayas: implication for models' wet bias over the Tibetan Plateau. *Clim. Dynam.* 51 (9–10), 3195–3207. <https://doi.org/10.1007/s00382-018-4074-x>.
- Lun, Y., Liu, L., Cheng, L., et al., 2021. Assessment of GCMs simulation performance for precipitation and temperature from CMIP5 to CMIP6 over the Tibetan Plateau. *Int. J. Climatol.* 41 (7), 3994–4018. <https://doi.org/10.1002/joc.7055>.
- Liu, L.Y., Wang, X.J., Gou, X.H., et al., 2022. Projections of surface air temperature and precipitation in the 21st century in the Qilian Mountains, Northwest China, using REMO in the CORDEX. *Adv. Clim. Change Res.* 13 (3), 344–358. <https://doi.org/10.1016/j.accre.2022.03.003>.
- Miao, Y., Wang, A., 2020. A daily $0.25^\circ \times 0.25^\circ$ hydrologically based land surface flux dataset for conterminous China, 1961–2017. *J. Hydrol.* 590, 125412. <https://doi.org/10.1016/j.jhydrol.2020.125413>.
- Mukul Tewari, N., Tewari, M., Chen, F., et al., 2004. Implementation and verification of the unified NOAA land surface model in the WRF model (Formerly Paper Number 17.5). *Proceedings of the 20th Conference on Weather Analysis and Forecasting/16th Conference on Numerical Weather Prediction (Seattle, USA)*.
- Muñoz-Sabater, J., Dutra, E., Agustí-Panareda, A., et al., 2021. ERA5-Land: a state-of-the-art global reanalysis dataset for land applications. *Earth Syst. Sci. Data* 13 (9), 4349–4383. <https://doi.org/10.5194/essd-13-4349-2021>.
- Niu, X., Tang, J., Chen, D., et al., 2021. Elevation-dependent warming over the Tibetan plateau from an ensemble of CORDEX-EA regional climate simulations. *J. Geophys. Res. Atmos.* 126, e2020JD033997. <https://doi.org/10.1029/2020jd033997>.
- Ou, T., Chen, D., Chen, X., et al., 2020. Simulation of summer precipitation diurnal cycles over the Tibetan Plateau at the gray-zone grid spacing for cumulus parameterization. *Clim. Dynam.* 54 (7–8), 3525–3539. <https://doi.org/10.1007/s00382-020-05181-x>.
- Ou, T., Chen, D., Tang, J., et al., 2023. Wet bias of summer precipitation in the northwestern Tibetan Plateau in ERA5 is linked to overestimated lower-level southerly wind over the plateau. *Clim. Dynam.* 61 (5–6), 2139–2153. <https://doi.org/10.1007/s00382-023-06672-3>.
- Prein, A.F., Ban, N., Ou, T., et al., 2023. Towards ensemble-based kilometer-scale simulations over the third pole region. *Clim. Dynam.* 60 (11), 4055–4081. <https://doi.org/10.1007/s00382-022-06543-3>.
- Shi, Y., Gao, X., Zhang, D., et al., 2011. Climate change over the Yarlung Zangbo–Brahmaputra River Basin in the 21st century as simulated by a high resolution regional climate model. *Quat. Int.* 244 (2), 159–168. <https://doi.org/10.1016/j.quaint.2011.01.041>.
- Shin, H., Hong, S., 2013. Analysis of resolved and parameterized vertical transports in convective boundary layers at gray-zone resolutions. *J.*

- Atmos. Sci. 70 (10), 3248–3261. <https://doi.org/10.1175/JAS-D-12-0290.1>.
- Skamarock, W.C., Klemp, J.B., Dudhia, J., et al., 2008. A description of the advanced research WRF version 3. NCAR Tech. Note 475, 113. <https://doi.org/10.13140/RG.2.1.2310.6645>.
- Sugimoto, S., Ueno, K., Fujinami, H., et al., 2021. Cloud-resolving-model simulations of nocturnal precipitation over the Himalayan slopes and foothills. *J. Hydrometeorol.* 22 (12), 3171–3188. <https://doi.org/10.1175/JHM-D-21-0103.1>.
- Wee, S.J., Park, E., Alcantara, E., et al., 2023. Exploring multi-driver influences on Indonesia's biomass fire patterns from 2002 to 2019 through geographically weighted regression. *J. Geovis. Spatial Anal.* 8 (1), 1–18. <https://doi.org/10.1007/s41651-023-00166-w>.
- Wang, D., Chen, Y., Jarin, M., et al., 2022. Increasingly frequent extreme weather events urge the development of point-of-use water treatment systems. *NPJ Clean Water* 5 (1). <https://doi.org/10.1038/s41545-022-00182-1>.
- Wang, X., Chen, D., Pang, G., et al., 2021a. Historical and future climates over the upper and middle reaches of the Yellow River Basin simulated by a regional climate model in CORDEX. *Clim. Dynam.* 56 (9), 2749–2771. <https://doi.org/10.1007/s00382-020-05617-4>.
- Wang, X., Chen, D., Pang, G., et al., 2021b. Effects of cumulus parameterization and land-surface hydrology schemes on Tibetan Plateau climate simulation during the wet season: insights from the RegCM4 model. *Clim. Dynam.* 57 (7–8), 1853–1879. <https://doi.org/10.1007/s00382-021-05781-1>.
- Wang, X., Pang, G., Yang, M., et al., 2016. Effects of modified soil water-heat physics on RegCM4 simulations of climate over the Tibetan Plateau. *J. Geophys. Res. Atmos.* 121 (12), 6692–6712. <https://doi.org/10.1002/2015jd024407>.
- Wang, X., Yang, M., Wan, G., et al., 2013. Qinghai–Xizang (Tibetan) Plateau climate simulation using the regional climate model RegCM3. *Clim. Res.* 57 (3), 173–186. <https://doi.org/10.3354/cr01167>.
- Wu, J., Gao, X., 2013. A set of gridded daily observational data for China and its comparison with other data. *Chin. J. Geophys.* 56 (4), 1102–1111. <https://doi.org/10.6038/cjg20130406> (Chinese).
- Xu, J., Koldunov, N., Remedio, A.R.C., et al., 2018. On the role of horizontal resolution over the Tibetan Plateau in the REMO regional climate model. *Clim. Dynam.* 51 (11–12), 4525–4542. <https://doi.org/10.1007/s00382-018-4085-7>.
- Zhu, Y., Lin, Z., Wang, J., et al., 2016. Impacts of climate changes on water resources in Yellow River Basin, China. *Procedia Eng.* 154, 687–695. <https://doi.org/10.1016/j.proeng.2016.07.570>.
- Zhang, Y., Yan, D., Wen, X., et al., 2019. Comparative analysis of the meteorological elements simulated by different land surface process schemes in the WRF model in the Yellow River source region. *Theor. Appl. Climatol.* 139 (1–2), 145–162. <https://doi.org/10.1007/s00704-019-02955-0>.
- Zhang, Z., Wang, X., Yang, M., et al., 2023. Spatio-temporal changes of key climatic elements in the upper Yellow River water conservation area in recent 60 years. *Plateau Meteorol.* 42 (9), 1372–1385 (Chinese). <https://doi.org/10.7522/j.issn.1000-0534.2023.00011>.